Miniature fiber-optic micro-flowmeter based on Fabry-Perot interferometer and carbon nanotubes

Weinan Liu, Shengli Pu, *Senior Member*, *IEEE*, Simiao Duan, Zijian Hao, Chencheng Zhang, and Qiang Wu

***Abstract*—A novel fiber-optic micro-flowmeter based on a Fabry-Perot interferometer (FPI) and carbon nanotubes (CNTs) has been proposed and investigated. The proposed sensor integrates a Fabry-Perot cavity on the tip of a single-mode fiber (SMF), which is used as the sensing probe. The Fabry-Perot cavity comprises an SMF and a short hollow-core fiber (HCF) section. The HCF is partially filled with CNTs-doped polydimethylsiloxane (CNTs-PDMS), which emits heat obviously due to the excellent photothermal effect of CNTs-PDMS when illuminated by a laser. Under a certain flow velocity, the heat would be taken away by a microfluid as it flows over the surface of the Fabry-Perot cavity until the thermal equilibrium is established. Besides, due to the thermal expansion of CNTs-PDMS, the variation of heat will result in a change in the cavity length of FPI. By monitoring the dip wavelength variation of the sensor, the microflow rate will be determined. The experimentally measured maximum flow rate sensitivity is 68.52 nm/(μL/s) in the 0-2 μL/s range. The proposed sensing probe is ultracompact, and the footprint is extremely small (the length of the sensing part is only 126 μm), which has potential in flow rate detection in narrow spaces and *in vivo* applications in biomedicine.**

***Index Terms*—Fabry-Perot interferometer, flowmeter, microfluid, fiber sensor.**

I. INTRODUCTION

FLOW rate is a vital parameter in micro total analysis systems in microfluidics, which is critical in various fields, including drug research, clinicopathological analysis, biosensing, and chemical analysis [1], [2], [3], [4]. For instance, flow rate dominates cell adhesion and monoclonal antibody production in drug research testing [5] and affects the speed and efficiency of counting and sorting in flow cytometry [6]. Traditional microflow rate monitoring methods include microelectromechanical systems (MEMS) and particle image velocimetry (PIV). MEMS-based flow rate sensors, which primarily utilize cantilever deflection [7], electrical admittance [8], [9], and thermal transfer [10], [11], offer high sensitivity but involve highly complex fabrication processes and are unsuitable for confined spaces due to their shape and relatively large size. PIV-based flow rate sensors require the fluid to be seeded with tracer particles, considerably complicating the measurement process and making them less suitable for real-time monitoring in certain biomedical applications [12], [13].

Fiber-optic flow rate sensors have emerged as a promising alternative, offering easy integration, low cost, compact size, and resistance to chemical erosion. Technologies for fiber-optic flow rate sensing include cantilever deflection [14], laser Doppler velocimeter (LDV) [15], and "hot wire" [16]. Cantilever sensors are based on the pressure caused by the fluid flow, which physically deforms the fiber sensor. According to this mechanism, Qiao *et al.* proposed a flowmeter based on fiber Bragg grating (FBG) [17]. Nevertheless, it is inevitable that the flow, to some extent, would be obstructed by the cantilever. LDV sensors have the obvious advantage of non-invasive measurement. However, the operation relies on the particles in the flow field to reflect the signal, which is unsuitable for some fluids. "Hot wire" sensors take advantage of a certain temperature difference between the probe and the surrounding environment and heat transfer. The fluid takes away more heat as the flow velocity increases, and the spectral shift is more pronounced. Following this guide, Liu *et al.* proposed a flowmeter based on high-light-absorption Co^{2+}-doped optical fiber [18]. The Co^{2+}-doped fiber absorbs light and generates heat. The central wavelength of the heated FBG will shift due to the thermally induced change of refractive index (RI) and grating period. Yan *et al.* proposed a flowmeter based on a gold-coated optical microfiber coupler (MC) [19]. The gold film absorbs the evanescent field of the MC, and then the generated heat warms the MC. However, most of these reported flow sensors do not have a sufficient spatial resolution to probe microfluid due to the excessive size (usually length >10 mm).

Carbo nanotubes (CNTs) are well-known nanomaterials with broadband absorption and high photothermal conversion efficiency [20]. The thermal conductivity of CNTs far surpasses that of metal materials. In addition, polydimethylsiloxane (PDMS) is a low-cost optical rubber material with non-toxic features, good light transmittance, excellent chemical stability, high thermo-optical coefficient (TOC) (-4.66×10^{-4}), and large thermal expansion coefficient (TEC) (9.6×10^{-4}) [21], [22].

This work was jointly supported by the National Natural Science Foundation of China (Grant No. 62075130), the Natural Science Foundation of Shanghai (Grant No. 23ZR1443300), and the Program of Shanghai Academic Research Leader (Grant No. 23XD1402200). *(Corresponding author: Shengli Pu).*

Weinan Liu, Simiao Duan, Zijian Hao, and Chencheng Zhang are with the College of Science, University of Shanghai for Science and Technology, Shanghai 200093, China (e-mail: 2448171287@qq.com).

Shengli Pu is with the College of Science, University of Shanghai for Science and Technology, and the Shanghai Key Laboratory of Modern Optical System, University of Shanghai for Science and Technology, Shanghai 200093, China (e-mail: shlpu@usst.edu.cn).

Qiang Wu is with the Department of Mathematics, Physics and Electrical Engineering, Northumbria University, NE1 8ST, United Kingdom (e-mail: qiang.wu@northumbria.ac.uk).

Color versions of one or more of the figures in this article are available online at http://ieeexplore.ieee.org

Therefore, it is particularly suitable as a sensitization material for temperature-dependent sensors. The interference from the thermo-optic effect of PDMS can be avoided when light does not enter the PDMS, as demonstrated by Kacik et al. in their optical fiber sensor based on an air microcavity in PDMS [23].

Considering these, a novel reflection-type flow rate sensing probe is proposed in this work. It comprises a single-mode fiber (SMF) end fused with a short hollow-core fiber (HCF) section. The HCF tip is partially filled with a mixture of PDMS and CNTs to form an air-cavity Fabry-Perot interferometer (FPI). CNTs are photothermal conversion elements that absorb light from lasers and generate heat. The air cavity length of FPI changes due to the thermal expansion of CNTs-doped PDMS (CNTs-PDMS). The fluid takes the heat away, and the shift of FPI dips enables flow rate sensing. Due to the filler of the cavity being air, the sensor is not affected by the thermo-optical effect of PDMS, in theory. Therefore, such a sensor has high spectral stability and then high sensitivity. The probe is ultracompact with a sensing area length of only 126 μm. So, it is suitable for microflow rate detection in narrow spaces and *in vivo* application in biomedicine. The proposed micro-flowmeter has great potential for application in drug research, hematology, oil prospecting, and ocean dynamics.

II. Sensing Principle and Simulations

The schematic diagram of the flow rate sensing probe is shown in Fig. 1. The sensor probe forms an air cavity (i.e., FPI) in the HCF, which is partially filled with CNTs-PDMS from the open end. Then, there are two reflective surfaces at the end of the SMF and the inside end of the CNTs-PDMS, labeled M_1 and M_2, respectively. In fact, the reflectivity of two reflective surfaces is low. Then, the FPI can be simplified as the configuration of double-beam interference. The CNTs within the CNTs-PDMS absorb the transmitted light. This scheme can ingeniously avoid the possible Vernier effect when the light reflection at the outside end of the CNTs-PDMS is considerable.

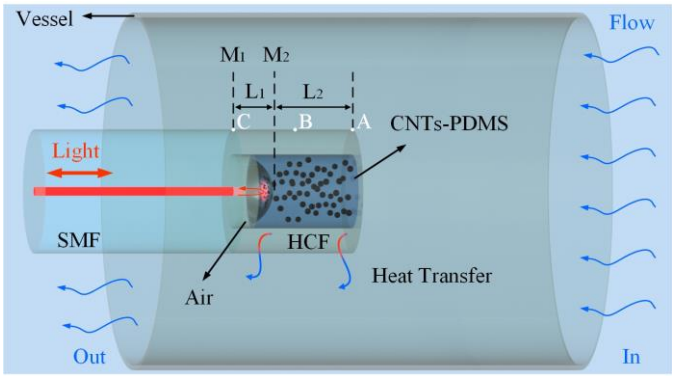

Fig. 1. Sensing structure of the flow rate sensing probe.

The reflection spectral function of FPI can be expressed as

$$I = I_1 + I_2 + 2\sqrt{I_1 I_2}\cos\left(4\pi n L_1 / \lambda\right), \quad (1)$$

where I is the reflected interference light intensity, I_1 and I_2 are the first and second reflected light intensities, respectively. λ is the wavelength of input light, L_1 is the cavity length, and n is the RI of the medium in the FPI cavity (air in our structure). According to (1), the effect of temperature on FPI spectrum can be expressed as

$$\frac{\Delta\lambda}{\Delta T} = \lambda\left(\frac{1}{n}\frac{\Delta n}{\Delta T} + \frac{1}{L_1}\frac{\Delta L_1}{\Delta T}\right), \quad (2)$$

where Δλ is the resonance wavelength shift of FPI, ΔT is the temperature change, ΔL_1 is the cavity length change, and Δn is the RI change of the air cavity. When the ambient temperature increases, the CNTs-PDMS will expand toward both ends equally. So, the variation of L_1 is half the expansion of CNTs-PDMS, that is $\Delta L_1 = -\Delta L_2/2$. Therefore, (2) can be rewritten as

$$\frac{\Delta\lambda}{\Delta T} = \lambda\left(\frac{1}{n}\frac{\Delta n}{\Delta T} - \frac{1}{2L_1}\frac{\Delta L_2}{\Delta T}\right) = \lambda\left(\frac{1}{n}\alpha - \frac{L_2}{2L_1}\beta\right), \quad (3)$$

where ΔL_2 is the length change of CNTs-PDMS, α is the TOC of air (-4.46×10^{-8}/°C), and β is the TEC of CNTs-PDMS. Considering that $\alpha \ll \beta$, we can obtain

$$\Delta\lambda = -\lambda\beta\frac{L_2}{2L_1}\Delta T . \quad (4)$$

The above equation reveals that the FPI dips shift towards shorter wavelengths with temperature increase. The advantage of this sensing structure is that it avoids the influence of the thermo-optic effect of PDMS. In addition, the air cavity will reduce the heat propagation along the optical fiber so that the heat is "confined" radially and is effectively transferred to the fluid to the maximum extent, which improves the sensitivity of the sensor. In contrast, if PDMS (or CNTs-PDMS) is used as the filling medium in the whole cavity (that is, fully filled), the thermo-optic effect and thermal expansion effect of PDMS will cause the FPI dips to shift in opposite directions, which is assigned to the TOC of PDMS is negative, but its TEC is positive. This will definitely result in reduced sensor sensitivity. Even worse, the spectral shift is unstable, and then it is not easy to monitor, and the response time is relatively longer.

During sensing scenarios, CNTs within CNTs-PDMS absorb laser light and generate heat. The temperature of CNTs-PDMS increases, and then the corresponding length (L_2) increases. When microfluid flows through the probe, it removes some heat. This leads to the contraction of CNTs-PDMS (i.e., L_2 decreases) and then the effective "expansion" of the air cavity (i.e., L_1 increases). Thus, the reflective spectrum will shift towards longer wavelengths according to Eq. (4). The heat loss (Q) depends on the flow rate, which can be given as [24]

$$Q = \left(A + Bv^m\right)\Delta T , \quad (5)$$

where *v* is the microfluidic flow rate. *A*, *B*, and m are empirical constants for a specific fluid and microfluidic channel condition (size, roughness, etc.). By combining (4) and (5), the resonance wavelength of FPI as a function of flow rate can be derived as

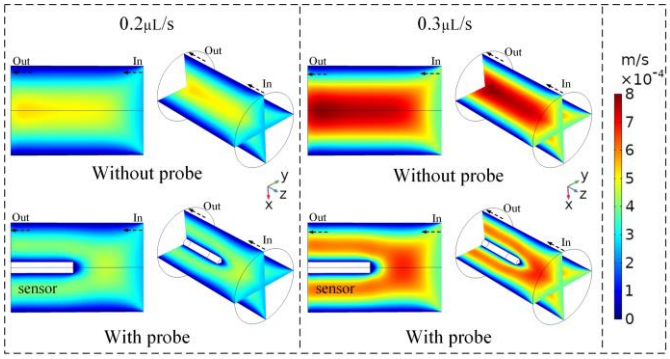

Fig. 2. Distribution of speed field under different flow rates for the cases with and without probe inserted in a channel.

$$\Delta\lambda = -\lambda\beta \frac{L_2}{2L_1} \frac{Q}{\left(A + Bv^m\right)}. \quad (6)$$

In fact, the measured flow rate within the channel is an average one. There are differences in flow speed at different locations in the channel. Moreover, the insertion of the sensing probe inevitably affects the local flow field. To clarify this, the local flow field at different ambient flow rates is simulated with COMSOL for the cases with and without a probe inserted in the channel, as shown in Fig. 2. The diameter of the channel is set at 1000 μm. The flow speed in the center of the channel is higher than those on both sides, and the flow speed near the channel wall is almost zero. Therefore, during our experiments, a three-dimensional displacement stage controls the probe to be as central as possible in the channel.

CNTs-PDMS is heated by a laser and can be considered as a heat source therein. Temperature distributions and heat flux streamlines at different flow rates are also simulated. For simulations, the overall length of the probe is set at 120 μm. The outer and inner diameters of the probe are 125 and 75 μm, respectively. The air and CNTs-PDMS cavity lengths are set to 40 and 80 μm (i.e., L_1 and L_2), respectively. The simulation results are shown in Fig. 3, which indicate that the sensors can finally reach thermal equilibrium at different flow rates. As

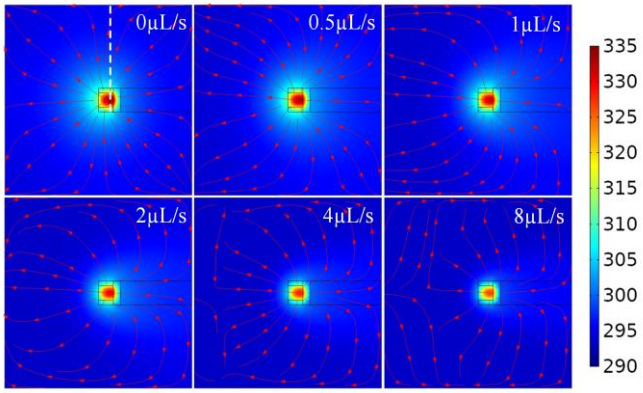

Fig. 3. Distribution of temperature field in a channel under different flow rates.

the flow rate increases, the thermal equilibrium temperature of the probe decreases significantly.

Fig. 4(a) gives the equilibrium temperature at three marked points (A, B, and C, which are the front, middle, and rear end of the outer wall of the probe, respectively (see Fig. 1)) at different flow rates. The overall trend of the three fitting curves is the same. The temperature changes slowly with the flow rate when the flow rate is relatively large. Since position C is not in direct contact with the heat source, its temperature is lower than those of the other two positions at 0 μL/s. A slight increase in the temperature with flow rate at position C at a low flow rate regime is assigned to the heat carried by the flow of the microfluid. Fig. 4(b) plots the temperature distribution across the cross-section of the channel (corresponding to the dashed line plotted in Fig. 3) at different flow rates. At distances larger than 337.5 μm from the probe, the temperature remains constant. Constant temperature means no more heat exchange. The higher the flow rate, the shorter the distance to temperature stabilization. Therefore, the sensor can detect the flow rate in the range smaller than 337.5 μm, which indicates that the sensor has ultra-high spatial resolution.

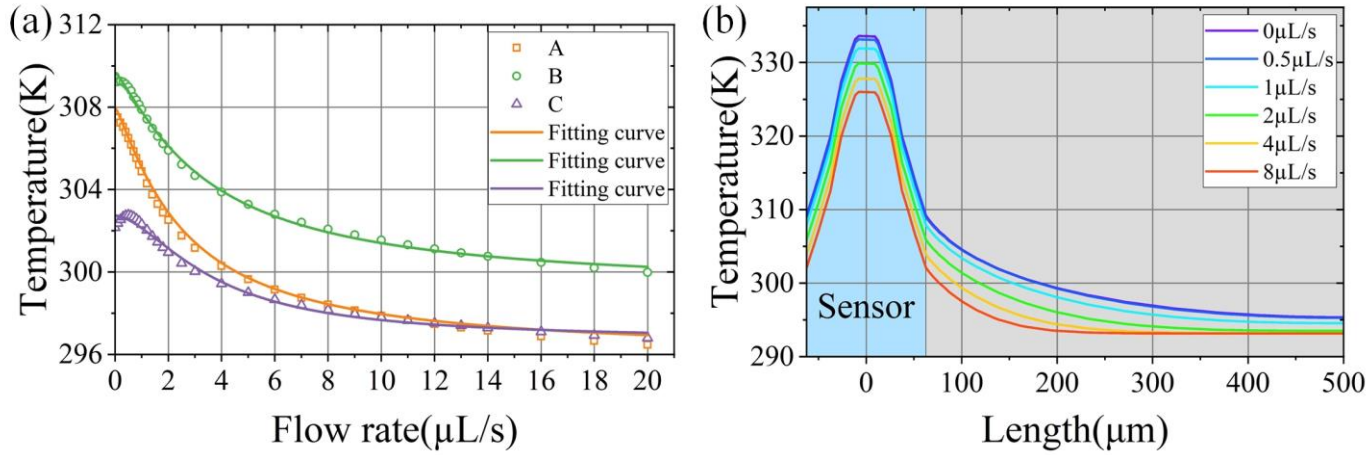

Fig. 4. Simulation results of equilibrium temperature of the flowmeter: (a) equilibrium temperature vs flow rate at three positions, and (b) distribution of equilibrium temperature across the cross-section of the channel at different flow rates.

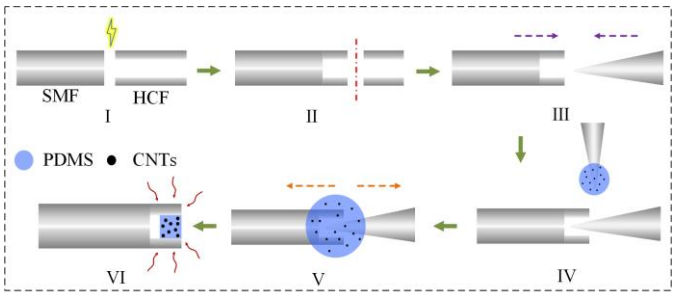

Fig. 5. Fabrication processes of the sensing probe.

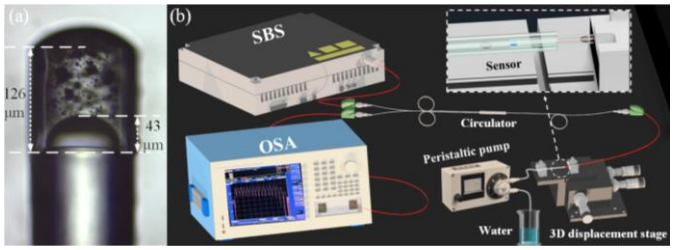

Fig. 6. Micrograph of the as-fabricated probe (a) and schematic diagram of the experimental setup for investigating the sensing properties (b).

III. Experiments and Sensing Performance

The fabrication processes of the sensing probe are illustrated in Fig. 5. First (step I), the HCF is spliced with the lead-in SMF using a fusion splicer (FSM-80C+, Fujikura). To avoid the collapse of the HCF air hole while ensuring a strong and reliable splice between the HCF and SMF, the fusion time is set to 400 ms, and the fusion power is -20 bit. HCF's inner and outer diameters are 75 and 125 μm, respectively. Second (step II), the HCF is cut with a remanent length of 126 μm using a fiber cleaver under a CCD camera. Then (step III), a tapered fiber is inserted into the HCF. Another tapered fiber is used to dip the CNTs-PDMS and drop it on the HCF termination (step IV). The PDMS solution is prepared by mixing the elastic polymer (Sylgard 184-A) and the curing agent (Sylgard 184-B) with a ratio of 10:1. The CNTs (multi-walled carbon nanotubes with an average diameter of 8-15 nm and a length of 3-12 μm) are doped into the PDMS solution at a mass ratio of 1% to obtain the CNTs-PDMS. Next (step V), the tapered fiber is pulled out of the HCF, and the CNTs-PDMS is sucked into the HCF due to the pressure. The inner surface of the CNTs-PDMS is concave and very smooth due to the surface tension of the CNTs-PDMS solution. Finally (step VI), the sensing probe is obtained after baking for 2 h at 80 °C in a column oven (LCO 102 LONG, ECOM Ltd., Czech Republic). The length of the air cavity is 43 μm after CNTs-PDMS curing (see Fig. 6(a) for the as-fabricated probe).

The experimental setup employed for investigating the flow rate sensing properties of the as-fabricated device is shown in Fig. 6(b). The light from the supercontinuum broadband light source (SBS, Wuhan Yangtze Soton Laser Co., Ltd., Wuhan) is injected into the optical circulator through Port 1 of the circulator. Then, it is transmitted into the probe through Port 2 of the circulator. The sensing light is reflected by the probe and transmitted to the optical spectral analyzer (OSA, Yokogawa AQ6370C) through Port 3 of the circulator. A three-dimensional displacement stage controls the probe to be placed in the center of the channel (channel diameter is 1 mm). A peristaltic pump is used to control the flow rate in the channel.

The following experiments were carried out at room temperature. The typical reflectance spectra of the sensor are illustrated in Fig. 7(a). When the power of the input laser increases, the spectrum is blue-shifted. Conversely, when the power of the input laser decreases, the spectrum is red-shifted. When the laser power increases, the CNTs within the CNTs-PDMS composite absorb more light, leading to increased heat generation due to their excellent photothermal conversion efficiency. This heat causes thermal expansion of the CNTs-PDMS, resulting in a change in the Fabry-Perot cavity length, which in turn shifts the reflectance spectrum. The spectral response to laser power is consistent with Eq. (4). The corresponding spatial spectrum obtained by the Fast Fourier Transform (FFT) of the reflectance spectrum is shown in Fig. 7(b). Peak 1, corresponding to the air cavity, significantly influences the reflectance spectrum.

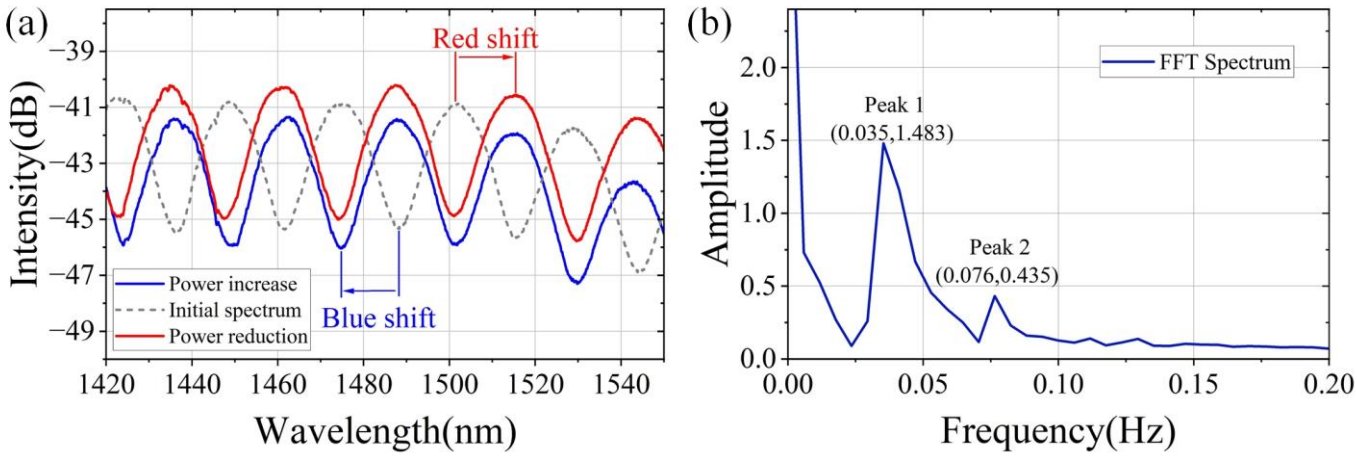

Fig. 7. Spectral response of the as-fabricated sensor: (a) response of reflectance spectrum to laser power and (b) FFT spectrum of the corresponding spectrum.

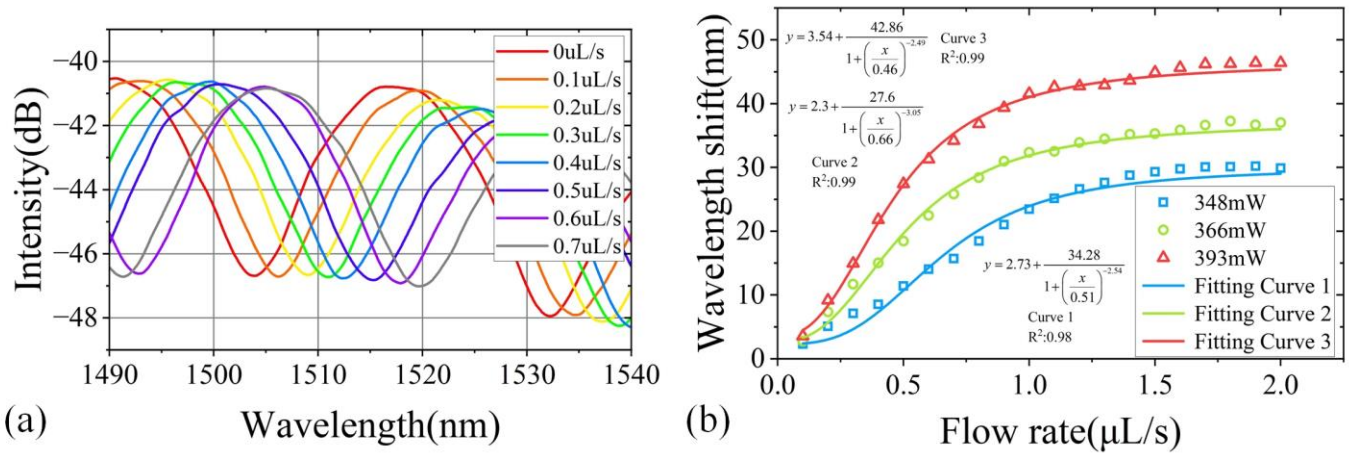

Fig. 8. Flow rate response of the as-fabricated sensor: (a) response of reflectance spectrum to flow rate and (b) relationship between wavelength shift and flow rate.

Fig. 8(a) shows the spectral response of the proposed sensor to flow rate at the laser power of 348 mW. The reflectance spectrum has a significant red shift with the increase in flow rate, which is consistent with the theoretical prediction. This is due to the sensor's microfluid-flow-induced temperature reduction. The flow rate response results and fitting curves at different laser powers are shown in Fig. 8(b). The higher laser power causes higher temperature due to absorption by CNTs-PDMS, and thus, larger temperature variation due to the absorption of microfluid with the same flow rate, resulting in a larger wavelength shift and a higher sensitivity of the sensor. When the flow rate is increased to 1 μL/s, almost all of the heat is removed, and the wavelength shift with the flow rate almost reaches the saturation value. The obtained maximum flow rate sensitivity is 68.52 nm/(μL/s) at the laser power of 393 mW. For the 0.02 nm resolution of the spectrometer (OSA, Yokogawa AQ6370C) employed in our experiments, the detection limit is 0.29 nL/s. However, the detection limit is critically dependent on the employed spectrometer. Considering the 1 pm resolution of the typical commercial interrogator (e.g., SI720, Micron Optics, Inc.), the lowest detection limit is 14.59 pL/s.

The working principle of a “hot wire” flowmeter is based on the response to temperature. The temperature response of the as-fabricated sensor is shown in Fig. 9(a). The reflectance spectrum exhibits a regular blue shift with increasing temperature. The temperature sensitivity of the sensor is -4.99 nm/℃, which indicates that the as-fabricated sensor has a good temperature response. Fig. 9(b) shows the stability test of the sensor at different flow rates at room temperature. The experimental results show that the sensor has good stability. The resonance dip is slightly redshifted at the flow rate of 0 μL/s. Because the laser is not fully warmed up, the output power increases somewhat with time. Afterward, there is a small fluctuation in the test results when the flow rate is 0.4 μL/s and 0.8 μL/s. This is mainly due to the pulsatile flow provided by the peristaltic pump. Fluctuations in ambient temperature can also affect the test results. The large free spectral range of the interference dips may introduce errors during data acquisition. Minor vibrations of the sensor caused by the flow can affect the stability of the spectrum, thereby leading to measurement errors. With a laser power of 366 mW, three flow measurements were conducted to verify the sensor's repeatability. The test results are shown in Fig. 9(c).

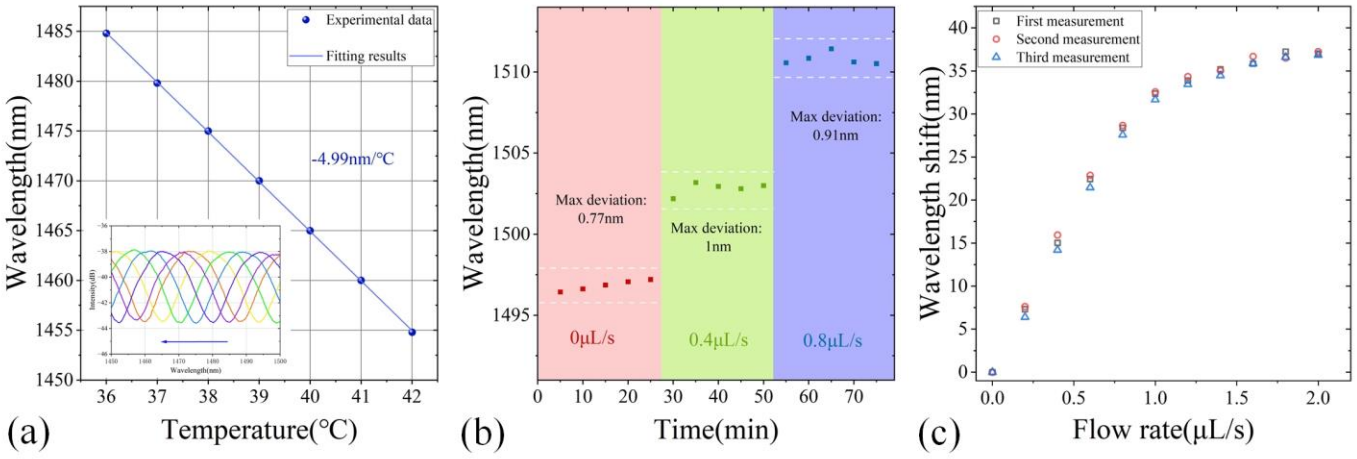

Fig. 9. Temperature response and stability test: (a) temperature-dependent reflectance spectra, (b) stability test under different flow rates and (c) repeatability test at the same laser power.

TABLE I
SENSING PERFORMANCE OF RELATED FIBER-OPTIC FLOW RATE SENSORS

Sensing structure	Type	Sensitivity	Size	Detection limit	Ref.
Microfiber coupler	Transmissive	2.183 nm/(μL/s)	About 1.2 mm*5 mm	9.2 nL/s	[19]
CO^{2+} doped fiber FPI	Transmissive	0.07 nm/(μL/s)	Over 500 μm*125 μm	285.7 nL/s	[25]
CO^{2+} doped micro FBG	Transmissive	0.31 nm/(μL/s)	30 mm*125 μm	64.5 nL/s	[18]
Micro FPI with silver nanoparticles	Reflective	1.5 nm/(μL/s)	300 μm*130 μm	80 nL/s	[26]
Micro FPI with CNTs	**Reflective**	**68.52 nm/(μL/s)**	**126 μm*125 μm**	**0.3 nL/s**	**This work**

The overall trend of the three measurement results is consistent, with no significant differences in sensitivity, only minor fluctuations. This indicates that the sensor has good repeatability.

For comparison, the performance indicators of the relevant sensing configurations are presented in Table 1. Compared with previous works on flow rate sensors, our work not only has ultra-high sensitivity but also has a compact configuration. In practical applications, sensing systems must consider the effects of ambient temperature, mechanical stability, manufacturing consistency, and biocompatibility. These factors are critical in ensuring reliable and accurate sensor performance across various environments and applications. Finally, owing to its simple manufacturing process and compact size, this sensor holds immense potential for extensive applications in the field of high-precision measurement of flow rate.

IV. CONCLUSION

In conclusion, an ultrasensitive micro-flowmeter based on FPI and CNTs is proposed and experimentally demonstrated. Due to the excellent photothermal performance of CNTs, the sensor has ultra-high sensitivity to flow rate. Experimental results demonstrate that the proposed sensor can achieve real-time in-situ micro-flow rate detection with ultra-high sensitivity, making it highly suitable for applications requiring precise measurement in narrow spaces. The sensor's compact size (126 μm in length) and high spatial resolution enable its use in biomedical in vivo applications, where traditional MEMS and PIV sensors are impractical due to their larger size and complex integration requirements. It is believed that this structure can provide a novel scheme for designing fiber-optic micro-flow rate sensing.

REFERENCES

[1] G. M. Whitesides, "The origins and the future of microfluidics," Nature, vol. 442, no. 7101, pp. 368-373, Jul. 2006.
[2] A. Manz, N. Graber and H. M. Widmer, "Miniaturized total chemical analysis systems: A novel concept for chemical sensing," Sens. Actuators, B, vol. 1, no. 1, pp. 244-248, Jan. 1990.
[3] M. Agostini and M. Cecchini, "Ultra-high-frequency (UHF) surface-acoustic-wave (SAW) microfluidics and biosensors," Nanotechnology, vol. 32, no. 31, pp. 312001, May. 2021.
[4] A. Mohan, P. Gupta, A. P. Nair, A. Prabhakar and T. Saiyed, "A microfluidic flow analyzer with integrated lensed optical fibers," Biomicrofluidics, vol. 14, no. 5, pp. 054104, Oct. 2020.
[5] J. H.-S. Kim, A. Marafie, X.-Y. Jia, J. V. Zoval and M. J. Madou, "Characterization of DNA hybridization kinetics in a microfluidic flow channel," Sens. Actuators, B, vol. 113, no. 1, pp. 281-289, Jan. 2006.
[6] W. Qin, L. Schmidt, X. Yang, L. Wei, T. Huang, J. Yuan, et al., "Laser guidance–based cell detection in a microfluidic biochip," Journal of Biomedical Optics, vol. 18, no. 6, pp. 060502, Jun. 2013.
[7] A. Quist, A. Chand, S. Ramachandran, D. Cohen and R. Lal, "Piezoresistive cantilever based nanoflow and viscosity sensor for microchannels," Lab Chip, vol. 6, no. 11, pp. 1450-1454, Nov. 2006.
[8] R. E. Oosterbroek, T. S. J. Lammerink, J. W. Berenschot, G. J. M. Krijnen, M. C. Elwenspoek and A. van den Berg, "A micromachined pressure/flow-sensor," Sens. Actuators, A, vol. 77, no. 3, pp. 167-177, Nov. 1999.
[9] J. Collins and A. P. Lee, "Microfluidic flow transducer based on the measurement of electrical admittance," Lab Chip, vol. 4, no. 1, pp. 7-10, Feb. 2004.
[10] M. Ashauer, H. Glosch, F. Hedrich, N. Hey, H. Sandmaier and W. Lang, "Thermal flow sensor for liquids and gases based on combinations of two principles," Sens. Actuators, A, vol. 73, no. 1, pp. 7-13, Mar. 1999.
[11] A. Glaninger, A. Jachimowicz, F. Kohl, R. Chabicovsky and G. Urban, "Wide range semiconductor flow sensors," Sens. Actuators, A, vol. 85, no. 1, pp. 139-146, Aug. 2000.
[12] M. D. Jeronimo, M. R. Najjari and D. E. Rival, "Echo-Lagrangian particle tracking: an ultrasound-based method for extracting path-dependent flow quantities," Meas. Sci. Technol., vol. 31, no. 5, pp. 054008, Feb. 2020.
[13] C. Yang, G. Luo, X. Yuan, J. Chen, Y. Lu, X. Tang, et al., "Numerical simulation and experimental investigation of multiphase mass transfer process for industrial applications in China," Rev. Chem. Eng., vol. 36, no. 1, pp. 187-214, Jun. 2020.
[14] M. S. Cheri, H. Latifi, J. Sadeghi, M. S. Moghaddam, H. Shahraki and H. Hajghassem, "Real-time measurement of flow rate in microfluidic devices using a cantilever-based optofluidic sensor," Analyst, vol. 139, no. 2, pp. 431-8, Jan. 2014.
[15] T. Tajikawa, W. Ishihara, S. Kohri and K. Ohba, "Development of miniaturized fiber-optic laser doppler velocimetry sensor for measuring local blood velocity: measurement of whole blood velocity in model blood vessel using a fiber-optic sensor with a convex lens-like tip," J. Sens., vol. 2012, pp. 426476, Jun. 2012.
[16] T. Zhang, T. Guo, R. Wang and X. Qiao, "A hot-wire flowmeter based on fiber Extrinsic Fabry–Pérot Interferometer with assistance of fiber Bragg grating," Opt. Commun., vol. 497, pp. 126952, Oct. 2021.
[17] X. Qiao, Q. Zhang, H. Fu and D. Yu, "Design of the target type flowmeter based on fiber Bragg grating and experiment," Chin. Opt. Lett., vol. 6, no. 11, pp. 815-817, Nov. 2008.
[18] Z. Liu, M.-L. V. Tse, A. P. Zhang and H.-Y. Tam, "Integrated microfluidic flowmeter based on a micro-FBG inscribed in Co2+-doped optical fiber," Opt. Lett., vol. 39, no. 20, pp. 5877-5880, Oct. 2014.
[19] S.-C. Yan, Z.-Y. Liu, C. Li, S.-J. Ge, F. Xu and Y.-Q. Lu, "Hot-wire" microfluidic flowmeter based on a microfiber coupler," Opt. Lett., vol. 41, no. 24, pp. 5680-5683, Dec. 2016.
[20] R. Singh and S. V. Torti, "Carbon nanotubes in hyperthermia therapy," Adv. Drug Delivery Rev., vol. 65, no. 15, pp. 2045-2060, Dec. 2013.
[21] M. P. Wolf, G. B. Salieb-Beugelaar and P. Hunziker, "PDMS with designer functionalities—Properties, modifications strategies, and applications," Prog. Polym. Sci., vol. 83, pp. 97-134, Aug. 2018.
[22] I. Turek, N. Tarjányi, I. Martinček and D. Káčik, "Effect of mechanical stress on optical properties of polydimethylsiloxane," Opt. Mater., vol. 36, no. 5, pp. 965-970, Mar. 2014.
[23] D. Kacik and I. Martincek, "Toluene optical fibre sensor based on air microcavity in PDMS," Opt. Fiber Technol., vol. 34, pp. 70-73. 2017.
[24] H. H. Bruun, "Hot-Wire Anemometry: Principles and Signal Analysis," Meas. Sci. Technol., vol. 7, no. 10, pp. 024, Oct. 1996.
[25] Y. Li, G. Yan, L. Zhang and S. He, "Microfluidic flowmeter based on micro "hot-wire" sandwiched Fabry-Perot interferometer," Opt. Express, vol. 23, no. 7, pp. 9483-93, Apr. 2015.
[26] J. Li, J. Qu, Y. Liu, Y. Li and S. Qu, "Novel fiber-tip micro flowmeter based on optofluidic microcavity filled with silver nanoparticles solutions," Nanophotonics, vol. 11, no. 21, pp. 4615-4625, Oct. 2022.

Weinan Liu was born in Liaoning, China, in 1998. He received a B.S. degree in physics from Shenyang Aerospace University, China, in 2020. He is currently pursuing a Ph.D. degree from the College of Science, University of Shanghai for Science and Technology, China.

His research interests include optical fiber interferometers, optical fiber processing, and sensing.

Shengli Pu (Senior Member, IEEE) received a Ph.D. degree from Shanghai Jiao Tong University in 2006. He was a Visiting Scholar with Cornell University from August 2012 to August 2013 and a Senior Research Fellow with Aalto University from July 2023 to September 2023.

He is currently a Professor at the College of Science, University of Shanghai for Science and Technology. He has co-authored over 150 peer-reviewed articles in physics and optics. His research interests include advanced photonic materials and devices, especially the novel optical properties and photonic applications of magnetic fluids/ferrofluids.

Simiao Duan was born in Chongqing, China, in 2000. She received her B.S. degree from the School of Physics and Electronic Engineering of Chongqing Normal University in 2021. She is currently studying for a master's degree from the School of Science of Shanghai University of Technology.

She is currently mainly engaged in research on high-sensitivity sensing technology.

Zijian Hao was born in 1996. He received a Ph.D. degree from the College of Science, University of Shanghai for Science and Technology, China.

He is currently working for a company that deals with physics.

Chencheng Zhang received a B.S. degree from Suzhou University of Science and Technology, China. She is currently pursuing a Ph. D. degree at the College of Science, University of Shanghai for Science and Technology.

Her current research interests are optical fiber processing and sensing.

Qiang Wu received the B.S. and Ph.D. degrees from Beijing Normal University and Beijing University of Posts and Telecommunications, Beijing, China, in 1996 and 2004, respectively. From 2004 to 2006, he worked as a Senior Research Associate at the City University of Hong Kong. From 2006 to 2008, he took up a research associate post at Heriot-Watt University, Edinburgh, U.K. From 2008 to 2014, he worked as a Stokes Lecturer at the Photonics Research Centre, Dublin Institute of Technology, Ireland.

He is with the Faculty of Engineering and Environment, Northumbria University, Newcastle Upon Tyne, United Kingdom; Key Laboratory of Opto-Electronic Information Science and Technology of Jiangxi Province, Nanchang Hangkong University. His research interests include optical fiber interferometers, nanofiber, and microsphere sensors for bio-chemical sensing.

He is an Editorial Board Member of Scientific Reports, an Associate Editor for IEEE Sensors Journal, and an Academic Editor for the Journal of Sensors.